




RESEARCH ARTICLE | MARCH 04 2024

Phase modulation by quantum gates of two microwave pulses in the framework of spin-boson model

Cheng Chen  ; Jiarui Zeng  ; Yao Yao  




J. Appl. Phys. 135, 094401 (2024)


<https://doi.org/10.1063/5.0195187>



CrossMark




Lock-in Amplifier



Boxcar Averager

Boost Your Optics and Photonics Measurements

 Zurich Instruments

[Find out more](#)

Phase modulation by quantum gates of two microwave pulses in the framework of spin-boson model

Cite as: J. Appl. Phys. 135, 094401 (2024); doi: 10.1063/5.0195187

Submitted: 31 December 2023 · Accepted: 16 February 2024 ·

Published Online: 4 March 2024



Cheng Chen,¹ , Jiarui Zeng,¹ and Yao Yao^{1,2,a)}

AFFILIATIONS

¹Department of Physics, South China University of Technology, Guangzhou 510640, China

²State Key Laboratory of Luminescent Materials and Devices, South China University of Technology, Guangzhou 510640, China

^{a)}Author to whom correspondence should be addressed: yaoyao2016@scut.edu.cn

ABSTRACT

As one of the most successful platforms of quantum control, trapped ions can be modulated by sequential microwave pulses to realize high-fidelity quantum logic gates, and dephasing noise may lead to invalidation of phase locking. In this work, we utilize the Dirac–Frenkel time-dependent variational approach with Davydov ansatz to simulate spin echo dynamics in the framework of spin-boson model. As the essential modulation parameters, pulse duration and waiting time have been comprehensively investigated to optimize the phase gates by two microwave pulses. We find that, as spin orientation undergoes periodic changes, the phase difference by acting one and two pulses exhibits spontaneous locking following time evolution, which indicates the robustness of the quantum phase gates. Spectrum of the environmental noise that is appropriate for the phase locking is also determined.

Published under an exclusive license by AIP Publishing. <https://doi.org/10.1063/5.0195187>

I. INTRODUCTION

Quantum simulation, as a computational paradigm, can extend the scope of classical computation in several research areas, including quantum chemistry,^{1–3} materials science,⁴ and even machine learning.^{5,6} Different from classical computers, quantum computers are based on the phase coherence in quantum mechanics to improve problem solving ability.⁷ A typical example is Shor's algorithm for factorization of integers based on the quantum Fourier transformation in which the phase coherence must be held long-term.⁸ Recent works have also developed quantum algorithms for building blocks and implementing quantum speedups in machine learning programs,^{9,10} such as the quantum basic linear algebra subroutines.^{11–14} However, it still poses considerable challenges in terms of hardware and software, especially the reservation of fidelity against thermal environment.

In recent years, numerous architectural systems for constructing quantum computing platform have made great progress, including ion traps,^{15,16} Rydberg atoms,^{17,18} color centers,^{19,20} quantum dots,^{21,22} superconducting qubits,^{23,24} and so on. Trapped ion quantum computing system is now capable of using >10 controllable connected qubits with high fidelity,^{25–27} even up to 50–100 ions

in some specific quantum analog systems.²⁸ Normally speaking, following quantum information processing, the dephasing of the associated qubits will be caused by the quasi-static inhomogeneity in the hopping frequency. Hahn echo sequences can coherently reverse this qubit evolution to counteract the effects of inhomogeneity and dephasing,²⁹ and most quantum phase gates are designed on this basis. For color centers in natural abundance ¹³C diamonds, e.g., the control of qubit phase can be achieved through microwave pulses, resulting in single-qubit phase gate times of ~50 ns and two-qubit gate times of ~1 μs.^{30,31} At low temperatures, the same sequence can be employed for optical state control as well.³² Recent work has successfully identified previously unrecognized narrow-band spectral noise features in the kinematic frequencies by tuning individual ¹⁷¹Yb⁺ ions captured in an ion trap with different optical wave sequences.³³ So far, the microwave modulation for phase gate has been used in systems such as ion traps, color centers, and molecular magnets, whose fidelity under the influence of a thermal environment has to be carefully investigated.

To comprehend the interplays between the microwave modulation and noise, we here conduct theoretical investigations in the

framework of the spin-boson model (SBM), because it has been demonstrated the classical noise can be described with a pure-dephasing boson bath.³⁴ The SBM is a benchmarking model to describe the influence of dephasing environments on a qubit, which depicts a two-level system coupled to a bath consisting of an infinite number of harmonic oscillators.^{35–38} The relevant coupling strength is normally described by the spectral function $J(\omega)$, which has got a relationship with the spectral exponent s given by $J(\omega) \sim \omega^s$. The dephasing bath can thus be classified as Ohmic ($s = 1$), sub-Ohmic ($s < 1$), and super-Ohmic ($s > 1$). For the Ohmic case, it is well-known that a transition occurs from a coherent phase to an incoherent phase, as well as a quantum phase transition from a delocalized phase to a localized phase. In addition, there are further developments based on the SBM such as the multistate harmonic model.³⁹ However, simulating the nonadiabatic quantum dynamics of the sub-Ohmic SBM accurately is always challenging due to the strong non-Markovian effects caused by the low-frequency bath modes. In the present paper, we introduce the variational Davydov ansatz for the simulations, which has been proved as a useful approach for the SBM and its quantum phase transition.^{40–44}

Furthermore, we take strong-coupling microwave pulses into account in our investigations. The strong-coupling external fields have gradually attracted attention in recent studies, exhibiting their unique applicability from the weak-coupling counterparts, such as far-off resonance excitations and informative non-linear optical responses beyond the limitations of pulse durations and transition dipole moments.^{45,46} It is demonstrated that the far-off resonance excitations in the strong pulse fields can be described with the Floquet–Landau–Zener (FLZ) theory, by developing the idea that the time evolution driven by the strong pulse fields can be regarded as adiabatic evolutions along with the instantaneous Floquet states and Landau–Zener-type diabatic transitions between them.⁴⁷ Motivated by the aforementioned works, it is interesting to introduce the strong external driving system into the spin-boson model to study the influence of strong pulses.

The paper is organized as follows. In Sec. II, we introduce the SBM with two microwave pulses and the Davydov D_1 Ansatz. Then we present numerical results and discuss the phase modulation by two microwave pulses under various conditions in Sec. III. Finally, conclusions are drawn.

II. METHODOLOGY

A. Model hamiltonian

In order to simulate the phase manipulation of quantum states in quantum logic gates, we introduce the idea of spin echo into the SBM by considering two sequential microwave pulses, as sketched in Fig. 1(a). The black arrow represents the qubit, and the wavy lines and balls describe the boson bath. We set coupling to the boson bath oriented in the z direction while rectangular microwave pulse in the x direction. The Hamiltonian of the total system is written as follows ($\hbar = 1$):

$$\hat{H} = \hat{H}_0 + \hat{H}_c(t), \quad (1)$$

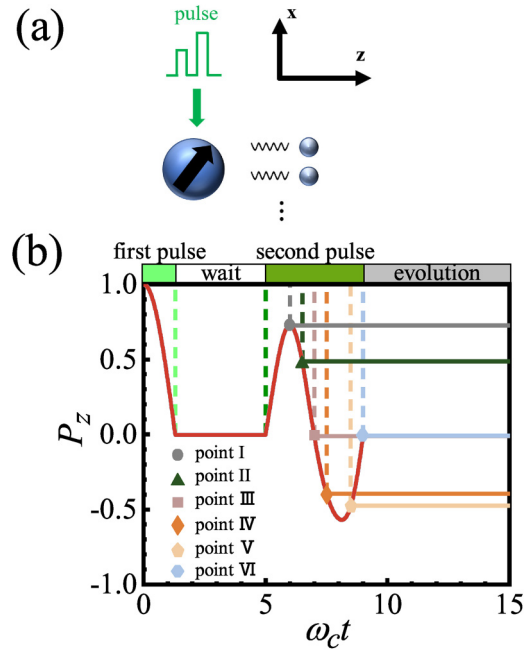


FIG. 1. (a) Schematic of the model. The wavy lines and balls represent the boson bath in the z direction, while the green polyline represents microwave pulses in the x direction. (b) Schematic of two microwave pulses modulation. The first pulse flips the spin from the $+z$ direction to the x - y plane. After the waiting time t_w , the duration between two pulses, the second pulse results in periodic oscillations of the spin orientation. In one period, we choose six special points I–VI as off points to switch off the second pulse.

where

$$\hat{H}_0 = -\frac{\Delta}{2}\hat{\sigma}_z + \omega_l \hat{a}_l^\dagger \hat{a}_l + \sum_k \omega_k \hat{a}_k^\dagger \hat{a}_k + \frac{1}{2}\hat{\sigma}_z \sum_k \lambda_k (\hat{a}_k + \hat{a}_k^\dagger) \quad (2)$$

and

$$\hat{H}_c(t) = \begin{cases} \Omega(t)\hat{\sigma}_x \{e^{-i\phi(t)}\hat{a}_l^\dagger + e^{i\phi(t)}\hat{a}_l\} & \text{pulse on,} \\ 0 & \text{pulse off.} \end{cases} \quad (3)$$

Here, $\hat{H}_c(t)$ represents the coupling of the rectangular microwave pulse to the system, with Rabi frequency $\Omega/\omega_c = 1$ and phase difference $\phi(t) = 0$ (for the first pulse) or $\phi(t) = \pi$ (for the second pulse). $\hat{\sigma}_z$ and $\hat{\sigma}_x$ are Pauli matrices referring to the spin. Energy splitting of the spin is adopted as $\Delta/\omega_c = 0.1$. \hat{a}_l^\dagger (\hat{a}_l) and \hat{a}_k^\dagger (\hat{a}_k) are creation (annihilation) operator of the microwave pulse and k th bosonic mode with frequency $\omega_k/\omega_c = 0.1$ and ω_k , respectively. λ_k is the coupling strength between the qubit and the k th bath mode, which is determined by a spectral density,

$$J(\omega) = \sum_k |\lambda_k|^2 \delta(\omega - \omega_k) = 2\alpha\omega_c^{1-s}\omega^s e^{-\omega/\omega_c}, \quad (4)$$

05 March 2024 01:10:33

with a spectral exponent s , cutoff frequency ω_c , and dimensionless constant α measuring the strength of the coupling. For practical simulations with the Davydov ansatz, $J(\omega)$ has to be discretized. We adopted the linear discretization method, and the coupling strength λ_k is written as $\sum_{k=1}^N \lambda_k^2 = \int_0^\infty d(\omega) J(\omega) \approx \sum_{k=1}^N J(\omega_k) \Delta\omega$.

In practice of spin echo technique, the phase of spin is modulated by adjusting the waiting time and duration of the second microwave pulse. Hence, the quantum dynamics evolution during and after pulse actions is also highly significant and worthy of attention. The schematic of pulse modulation and the population evolution $P_z(t)$ of the qubit are clearly showed in Fig. 1(b). Throughout the process, we choose two microwave pulses sequence that the first is first-pulse and the second is second-pulse with a waiting time t_w between them. We set the initial quantum state $|\Psi(0)\rangle = |+\rangle$, and the first-pulse flips the spin from the $+z$ direction to the x - y plane. Then the qubit stays in the plane during waiting as \hat{H} does not contain any flipping operator. The subsequent application of the second pulse refers to the reverse of time evolution by reversing the sign of the Hamiltonian, and thus a periodic oscillation and decay of the population $P_z(t)$ is observed, reflecting the echo dynamics of $\pm z$ directions. We are more concerning with the influence of different durations τ of the second-pulse on the phase evolution in both single-pulse and double-pulse scenarios. Therefore, within one period of the spin precession during the application of the second-pulse, we select six representative time points as the “off points” to switch off the second pulse, as indicated by I–VI in Fig. 1(b). Our rules of selections are described as follows. At first, we set a point as the “open point” to switch on the second pulse, and then choose two time points, at which the spin direction is first and second flipped to the x - y plane by the second pulse, as points III and VI. Then, we choose two points as points I and II, referring to 1/2 and 3/4 of the time interval between the open point and point III. Similarly, points IV and V correspond to 1/4 and 3/4 of the time interval between points III and VI. These off points serve as essential parameters for the phase modulation in both theories and experiments.

After acquiring the propagations of the model, we focus on the performance of phase locking and in-phase as well as out-of-phase synchronizations. The phase locking has become an important experimental technique of manipulations and detections of the quantum states in quantum optics and information,⁴⁸ such as multipartite entanglement,^{49–51} cluster states,^{52,53} etc. In the present investigations, phases of two evolution results should be equal within tolerance for the in-phase synchronization, while separated by 180° for the out-of-phase synchronization.⁵⁴ We adopt a measurement $|\Delta t| = |t_{\text{one}} - t_{\text{two}}|$ to describe the performance of the phase modulation. Herein, t_{one} and t_{two} are the time of extreme values nearest to a certain time point, of one- and two-pulse lines, respectively. For the out-of-phase synchronization, the measurement is labeled as $|\Delta t_{\text{out}}|$, with t_{one} (t_{two}) referring to the maximum (minimum) value. Then, smaller $|\Delta t_{\text{out}}|$ corresponds to better results of the out-of-phase synchronization. For the in-phase synchronization, both t_{one} and t_{two} represent the time of the maximum or minimum values and thus better results of the in-phase synchronization require a smaller measurement result, $|\Delta t_{\text{in}}|$. Corresponding sketches are shown in Fig. 2.

B. Time-dependent variational approach with Davydov Ansatz

In order to obtain the time evolution of the wave function $|\Psi(t)\rangle$ for the total Hamiltonian, it is a common practice to describe it through the Schrödinger equation. In the present paper, a time-dependent variational method based on coherent states, so-called Davydov D_1 ansatz, is adopted to solve the SBM. The D_1 ansatz can be written as^{40–42}

$$|D_s(t)\rangle = A(t)|+\rangle \exp \left[\sum_k \left(f_k(t) \hat{b}_k^\dagger - \text{h.c.} \right) \right] |0\rangle + B(t)|-\rangle \exp \left[\sum_k \left(g_k(t) \hat{b}_k^\dagger - \text{h.c.} \right) \right] |0\rangle, \quad (5)$$

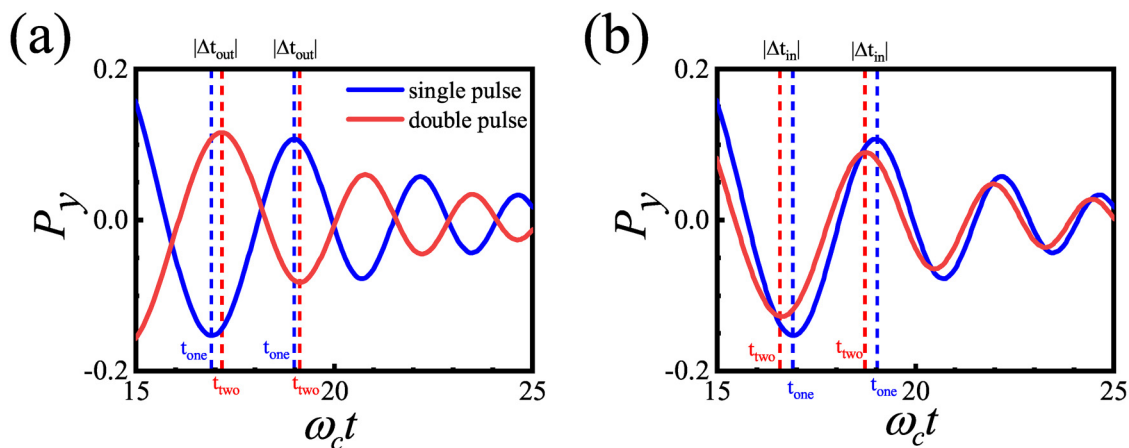


FIG. 2. Sketches of the values of (a) t_{one} , t_{two} , and $|\Delta t_{\text{out}}|$ for out-of-phase synchronization and (b) t_{one} , t_{two} , and $|\Delta t_{\text{in}}|$ for in-phase synchronization.

where $A(t)$ and $B(t)$ represent amplitudes of the states $|+\rangle$ and $|-\rangle$, respectively. $f_k(t)$ and $g_k(t)$ denote complex displacements of the k th bosonic mode, and $|0\rangle$ is the vacuum state of the boson bath.

Applying the Dirac–Frenkel time-dependent variational principle within the Lagrangian formalism, we can derive the time evolution equations for $A(t)$, $B(t)$, $f_k(t)$, and $g_k(t)$,

$$\frac{d}{dt} \frac{\partial L}{\partial \dot{u}_n^*} - \frac{\partial L}{\partial u_n^*} = 0, \quad (6)$$

where u_n^* represents the complex conjugate of the variational parameter u_n , which can be $A(t)$, $B(t)$, $f_k(t)$, or $g_k(t)$. The Lagrangian associated with the state $|D_s(t)\rangle$ is given by

$$L = \langle D_s(t) | \frac{i}{2} \frac{\partial}{\partial t} - \hat{H} | D_s(t) \rangle. \quad (7)$$

Combining Eqs. (5)–(7) and the Runge–Kutta method, we can obtain the time evolution of the variational parameters. Then physical observables of interest, expectation of $\hat{\sigma}_i$, can be acquired as

$$P_i(t) \equiv \langle \hat{\sigma}_i \rangle = \langle D_s(t) | \hat{\sigma}_i | D_s(t) \rangle, \quad (i = x, y, z). \quad (8)$$

Here, $P_x(t)$ and $P_y(t)$ describe the real and imaginary components of coherence, while $P_z(t)$ represents the overall difference. By substituting Eq. (5) into Eq. (8), one obtains

$$P_z(t) = |A|^2 - |B|^2, \quad (9)$$

$$P_x(t) = A^* B \exp \left\{ \sum_k \left[f_k^* g_k - \frac{1}{2} (|f_k|^2 + |g_k|^2) \right] \right\} + B^* A \exp \left\{ \sum_k \left[g_k^* f_k - \frac{1}{2} (|f_k|^2 + |g_k|^2) \right] \right\}, \quad (10)$$

and

$$P_y(t) = -iA^* B \exp \left\{ \sum_k \left[f_k^* g_k - \frac{1}{2} (|f_k|^2 + |g_k|^2) \right] \right\} + iB^* A \exp \left\{ \sum_k \left[g_k^* f_k - \frac{1}{2} (|f_k|^2 + |g_k|^2) \right] \right\}. \quad (11)$$

III. NUMERICAL RESULTS

In the following, we focus on the quantum dynamics of the phase modulation by two microwave pulses. The qubit is initially prepared in state $|+\rangle$ at $t = 0$, and we choose a factorized bath referring to a vacuum state with $f_k(0) = g_k(0) = 0$. In each simulation, we calculate both one- and two-pulse scenarios in parallel to observe whether the phase is locked, and for the former case the second pulse is absent which is just equivalent to the free induction decay.

A. Waiting time

Figure 3 displays the coherence dynamics of $P_y(t)$ for the spectral exponent $s = 0.25$ and coupling strength $\alpha = 0.01$ with respect to different waiting time t_w and duration time τ . The blue and red lines represent one- and two-pulse scenarios, respectively. With increasing τ showed as I–VI within one period, the oscillations of the red lines exhibit shift compared with the blue one. In particular, it manifests a retarded shift at off points I–III and advanced shift at points IV–VI. The results of the phase differences with respect to the duration time might be attributed to the strong-coupling pulses. It has been described that the strong system-field interactions can cause a sophisticated effective propagator by means of the non-perturbative response functions (NPRFs) and lead the evolutions of spectral peak intensities to phase retarded and advanced shifts in 2D spectroscopy.⁴⁶ In both investigations including ours, the phase manipulations under strong-coupling pulses can be regarded as level transitions and described in another representation, leading to adiabatic evolutions and diabatic transitions in the framework of the FLZ theory.⁴⁷ Therefore, it is our future scope to combine both NPRFs and FLZ theory for further investigations.

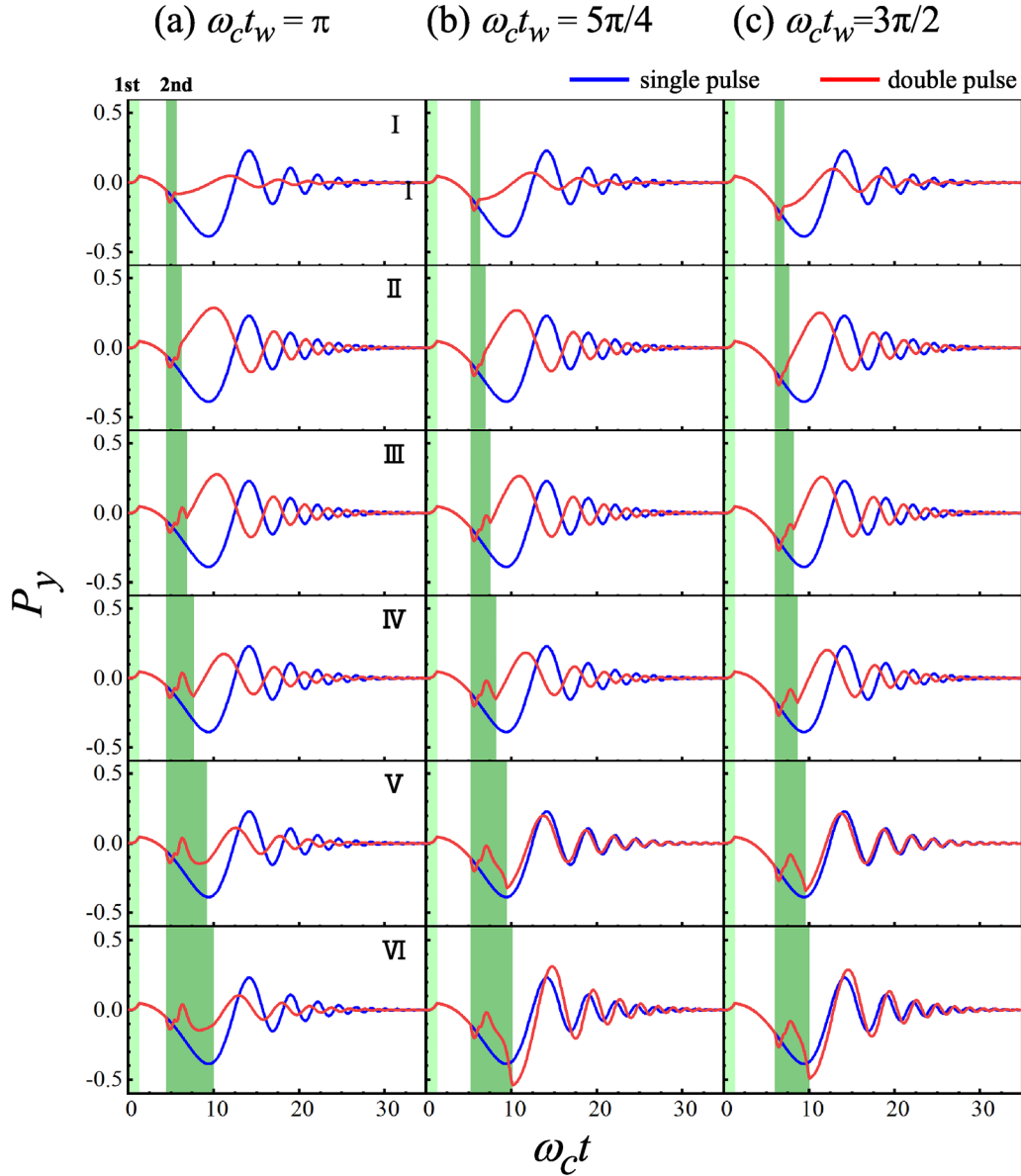
As a result, the phase difference between the red and blue lines distinctly illustrates the crossing from the out-of-phase to in-phase synchronization. We observe that during the flipping process from $+z$ to $-z$, as sketched in Fig. 1(b), the results are in the out-of-phase synchronization, whereas when the spin is flipped from $-z$ to the x – y plane, the results become in-phase synchronization. Moreover, it is found that the phase is spontaneously locked within $\omega_c t < 30$, indicating the phase gates are robust and can automatically adjust themselves with different pulse operations.

For quantum logic gates, we aim to get high-fidelity phase locking for both in-phase and out-of-phase manipulations. We thus calculate $|\Delta t_{\text{out}}|$ and $|\Delta t_{\text{in}}|$, at two off points III and V, respectively, to exhibit the influence of the waiting time t_w on the phase modulation by two microwave pulses, as illustrated in Fig. 4. We adopt a measurement $|\Delta t| = |t_{\text{one}} - t_{\text{two}}|$ to describe the performance of the phase modulation. Herein, both $|\Delta t_{\text{out}}|$ and $|\Delta t_{\text{in}}|$ are calculated from the time of the extreme values nearest to $\omega_c t = 30$. As shown in Fig. 4, the waiting time t_w has a significant influence on the performance of phase locking in both two cases. This is because the coherence is continuously evolving during waiting time, as “waiting” just refers to the population on the z -direction. The green shaded region in Fig. 4 therefore represents a preferable range for optimal waiting time to realize a robust phase modulation.

B. Dephasing bath

As mentioned in the Introduction, the noise can be modeled by a dephasing boson bath and the spectral function turns out to be essential. Here, in order to investigate how the thermal environment influences the phase modulation, we vary the spectral exponent s and coupling strength α to change the dephasing bath.

Figure 5 displays the dynamics of $P_y(t)$ for different dephasing bath of one and two pulses, respectively. The calculations here are performed with the waiting time $\omega_c t_w = 3.7$ and model parameters $\alpha = \{0.02, 0.03\}$ and $s = 0.25$ as well as $\alpha = 0.01$ and $s = \{0.5, 1, 1.5\}$, to discuss the influences of the bath. Despite the different thermal environments, overall, the shift of P_y in the



05 March 2024 01:10:33

FIG. 3. Quantum coherence dynamics of $P_y(t)$ for $s = 0.25$ and $\alpha = 0.01$, with (a) $\omega_c t_w = \pi$, (b) $\omega_c t_w = \frac{5\pi}{4}$, and (c) $\omega_c t_w = \frac{3\pi}{2}$. The green regions represent the duration of acting the first-pulse and the second-pulse, respectively. Patterns I–VI display the different duration τ of the second-pulse. Blue and red lines refer to one-pulse and two-pulse scenarios.

two-pulse scenario in Fig. 5 is similar to that in Fig. 3. The magnitude of this shift is closely related to the decay of the dephasing bath, as shown in Figs. 5(a) and 5(b). As the environmental decay increases, P_y in the two-pulse scenario slightly changes, and the out-of-phase phenomenon is almost absent at off point III. On the contrary, in Figs. 5(c) and 5(d), following the environmental decay decreases, the out-of-phase results at off point III and in-phase results at point V become more pronounced.

To further investigate the influence of the dephasing bath on phase modulation, we construct different dephasing baths by varying s and α . Numerical simulations are performed till the evolution time $\omega_c t = 20$, and $|\Delta t|$ at off points III and V, with the same definitions as Fig. 4, is calculated to characterize the phase coherence. Figure 6(a) illustrates that, at off point III, as s increases and α decreases, namely, the reduction of the decay of the dephasing bath, it tends to become out-of-phase synchronization, in

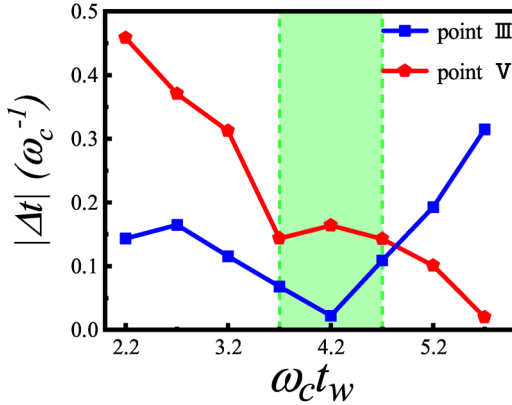


FIG. 4. $|\Delta t_{\text{out}}|$ at point III (blue lines) and $|\Delta t_{\text{in}}|$ at point V (red lines) with respect to the waiting time $\omega_c t_w$, both of which are acquired from the time of the extreme values nearest to $\omega_c t = 30$. Model parameters are $\alpha = 0.01$ and $s = 0.25$. The green shaded region denotes optimal waiting time for both out-of-phase and in-phase cases.

which α has a particularly strong influence. On the other hand, we also investigate the situation at off point V as shown in Fig. 6(b), where a decrease of the decay also makes it exhibit an oscillation shift, and we observe that it more likely to exhibit complete in-phase effect when $s = 0.25$ and $\alpha = 0.015$, $s = 1$ and $\alpha = 0.02$, or $s = 1.5$ and $\alpha = 0.025$.

C. From out-of-phase to in-phase

It is noticed for off point IV in Fig. 5, the coherence dynamics $P_y(t)$ crosses from the out-of-phase to in-phase synchronization in long-time scale. As exemplified in Figs. 7(a) and 7(b), after the second pulse, $P_y(t)$ exhibits a good out-of-phase result comparing with the one-pulse counterpart until about $\omega_c t = 30$. However, the coherence dynamics tends to be in-phase while further evolving. To determine the performance of the phase modulation, we here again calculate $|\Delta t_{\text{out}}|$ and $|\Delta t_{\text{in}}|$, and plot them in Figs. 7(c)–7(f). It is clearly seen for all considered scenarios, $|\Delta t_{\text{in}}|$ always decreases and approaches zero, confirming the above discussion of the crossing from the out-of-phase to in-phase synchronization. $|\Delta t_{\text{out}}|$ and $|\Delta t_{\text{in}}|$ intersect at about $\omega_c t = 35$, indicating the crossing occurs.

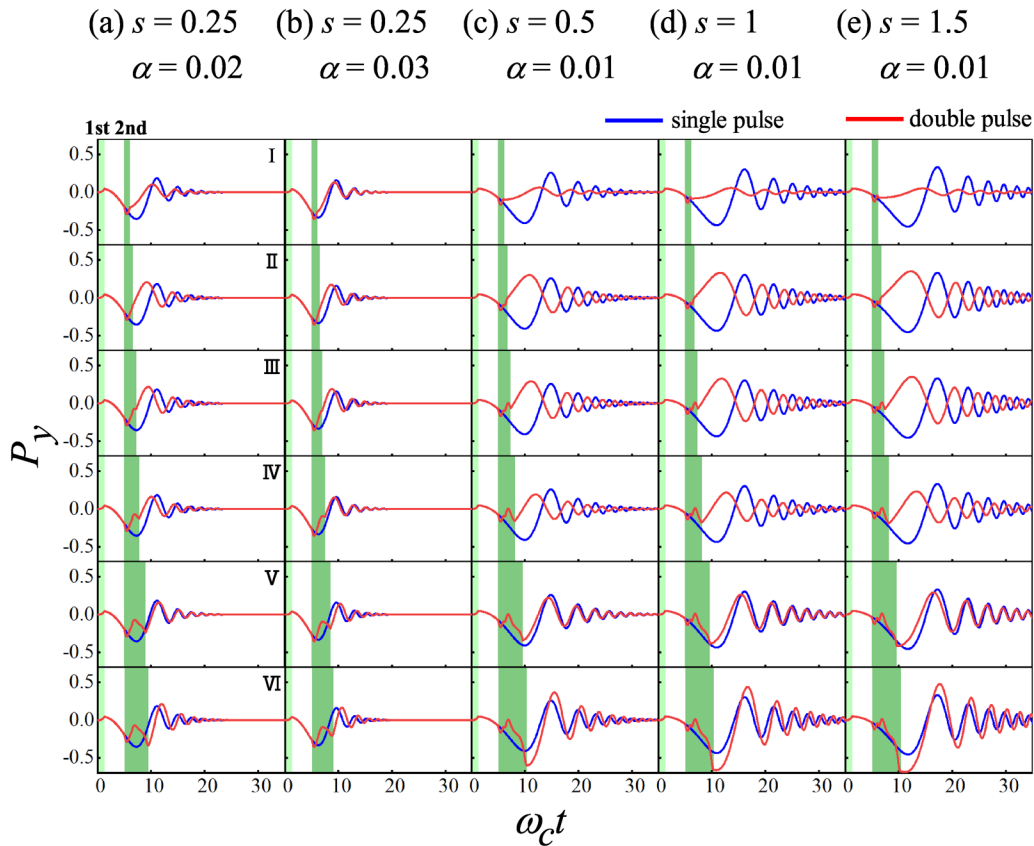


FIG. 5. Quantum coherence dynamics of $P_y(t)$ for (a) $s = 0.25$, $\alpha = 0.02$, (b) $s = 0.25$, $\alpha = 0.03$, (c) $s = 0.5$, $\alpha = 0.01$, (d) $s = 1$, $\alpha = 0.01$ and (e) $s = 1.5$, $\alpha = 0.01$, with $\omega_c t_w = 3.7$. The green regions represent the duration of the first-pulse and the second-pulse, respectively. Patterns I–VI display the different duration τ of the 2nd-pulse. Blue and red lines refer to one-pulse and two-pulse scenarios.

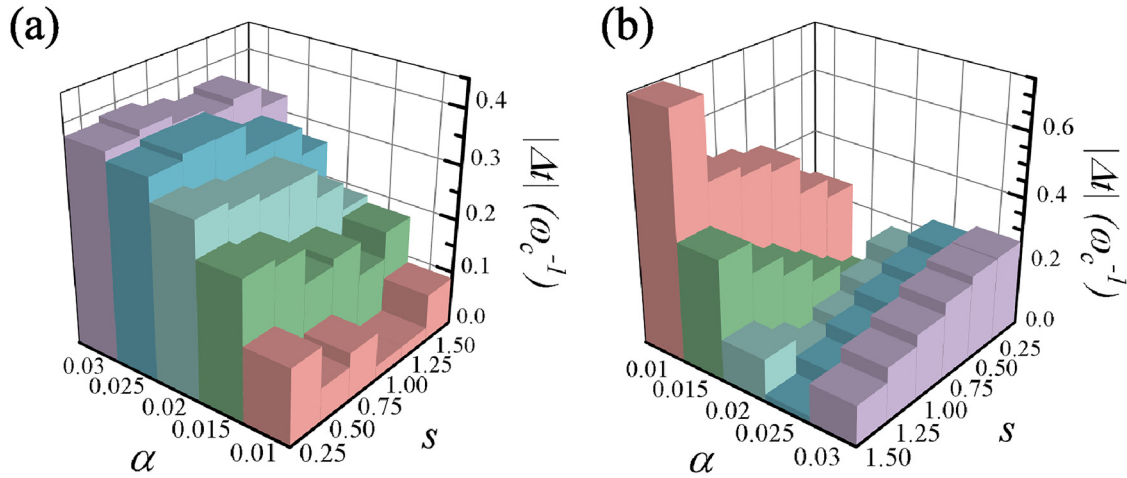


FIG. 6. (a) $|\Delta t_{\text{out}}|$ at point III and (b) $|\Delta t_{\text{in}}|$ at point V with respect to the model parameters α and s . Both of them are acquired from the time of the extreme values nearest to $\omega_c t = 20$. The waiting time $\omega_c t_w = 3.7$.

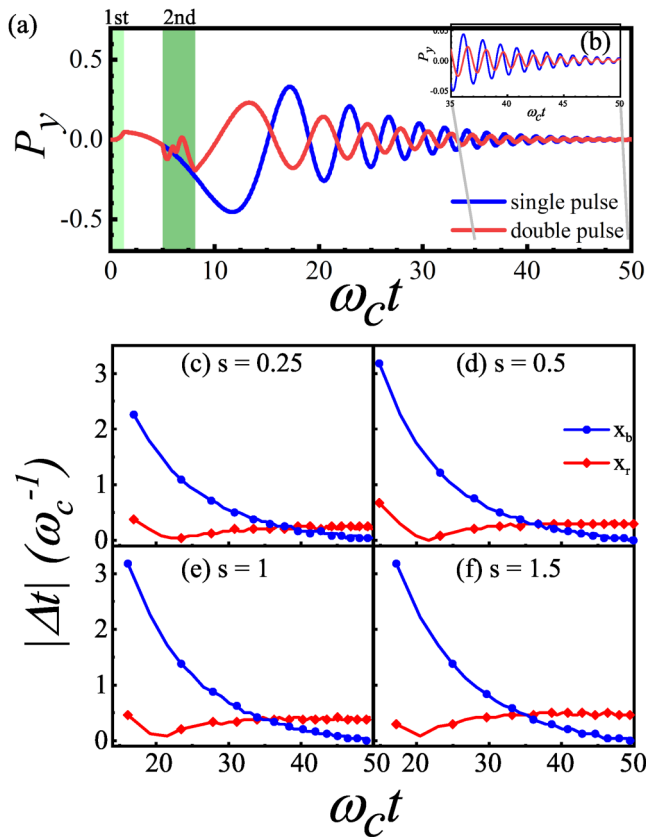


FIG. 7. (a) Quantum coherence dynamics $P_y(t)$ for $s = 1.5$ and $\alpha = 0.01$, with $\omega_c t_w = 3.7$ and at off point IV. (b) Detailed view of (a). (c)–(f) At off point IV, $|\Delta t_{\text{out}}|$ (red lines) and $|\Delta t_{\text{in}}|$ (blue lines) acquired from the time of the extreme values nearest to different $\omega_c t$. Model parameters are $\alpha = 0.01$ and $s = \{0.25, 0.5, 1, 1.5\}$.

Hence, we point out a critical time for the phase modulation to acquire a out-of-phase result at point IV. In addition, we find the model parameter has also influence on the crossing, exhibited as the critical time slightly delays with decreasing s .

IV. CONCLUSIONS

In summary, we have studied a model to introduce the echo dynamics into the SBM, achieving phase modulation through sequential microwave pulses. We apply the Dirac–Frenkel the time-dependent variational method with the Davydov D_1 ansatz for performing numerical simulations of phase modulation by one and two pulses. By analyzing the dynamics of quantum coherence P_y , we observe that the evolution of P_y with two pulses exhibits retarded and advanced shifts. We observe a phenomenon of phase locking in the coherence evolutions with a defined duration of the second pulse, which is correlated to the pulse interval and environmental dephasing. For a shorter pulse duration and weaker environmental dephasing, a clear tendency for the out-of-phase synchronization is found. On the contrary, for a longer pulse duration and stronger environmental dephasing, a tendency toward the in-phase synchronization is obtained. Quantum logic gates are normally subjected to various factors, including microwave pulse width and intervals. Our model simulates quantum phase modulation in quantum logic gates by extending the SBM with microwaves, providing practical implications for experiments. It is still a worthy direction for further research studies to focus on how to better simulate more complex and even real dephasing environment of quantum logic gates. Moreover, it is noticed the qubits have been treated as nanoprobe for the detection of noises,^{55–58} and recent endeavors have focused on investigating noise spectrum detection through the application of harmonic oscillators.^{33,59} Our proposed model may be extended to serve as nanoprobe in the above systems for noise detection, showcasing the potential for high-precision trapped-ion detection. We will next focus on these directions.

05 March 2024 01:10:33

ACKNOWLEDGMENTS

The authors gratefully acknowledge support from the National Natural Science Foundation of China (NNSFC) (Grant Nos. 12374107 and 11974118).

AUTHOR DECLARATIONS

Conflict of Interest

The authors have no conflicts to disclose.

Author Contributions

Cheng Chen: Conceptualization (supporting); Data curation (lead); Formal analysis (lead); Investigation (lead); Methodology (lead); Validation (equal); Writing – original draft (lead). **Jiarui Zeng:** Methodology (supporting); Validation (equal); Writing – review & editing (equal). **Yao Yao:** Conceptualization (lead); Supervision (lead); Writing – review & editing (equal).

DATA AVAILABILITY

The data that support the findings of this study are available from the corresponding author upon reasonable request.

REFERENCES

- ¹Y. Cao, J. Romero, J. P. Olson, M. Degroote, P. D. Johnson, M. Kieferová, I. D. Kivlichan, T. Menke, B. Peropadre, N. P. Sawaya *et al.*, *Chem. Rev.* **119**, 10856 (2019).
- ²S. McArdle, S. Endo, A. Aspuru-Guzik, S. C. Benjamin, and X. Yuan, *Rev. Mod. Phys.* **92**, 015003 (2020).
- ³I. Kassal, J. D. Whitfield, A. Perdomo-Ortiz, M.-H. Yung, and A. Aspuru-Guzik, *Ann. Rev. Phys. Chem.* **62**, 185 (2011).
- ⁴B. Bauer, S. Bravyi, M. Motta, and G. K.-L. Chan, *Chem. Rev.* **120**, 12685 (2020).
- ⁵J. Biamonte, P. Wittek, N. Pancotti, P. Rebentrost, N. Wiebe, and S. Lloyd, *Nature* **549**, 195 (2017).
- ⁶X.-D. Cai, D. Wu, Z.-E. Su, M.-C. Chen, X.-L. Wang, L. Li, N.-L. Liu, C.-Y. Lu, and J.-W. Pan, *Phys. Rev. Lett.* **114**, 110504 (2015).
- ⁷R. P. Feynman, *Int. J. Theor. Phys.* **21**, 467 (1982).
- ⁸P. W. Shor, in *Proceedings 35th Annual Symposium on Foundations of Computer Science (IEEE, 1994)*, pp. 124–134.
- ⁹M. Schuld, I. Sinayskiy, and F. Petruccione, *Contemp. Phys.* **56**, 172 (2015).
- ¹⁰P. Wittek, *Quantum Machine Learning: What Quantum Computing Means to Data Mining* (Academic Press, 2014).
- ¹¹A. W. Harrow, A. Hassidim, and S. Lloyd, *Phys. Rev. Lett.* **103**, 150502 (2009).
- ¹²N. Wiebe, D. Braun, and S. Lloyd, *Phys. Rev. Lett.* **109**, 050505 (2012).
- ¹³P. Rebentrost, M. Mohseni, and S. Lloyd, *Phys. Rev. Lett.* **113**, 130503 (2014).
- ¹⁴M. Schuld, I. Sinayskiy, and F. Petruccione, *Phys. Rev. A* **94**, 022342 (2016).
- ¹⁵C. D. Bruzewicz, J. Chiaverini, R. McConnell, and J. M. Sage, *Appl. Phys. Rev.* **6**, 021314 (2019).
- ¹⁶C. Monroe, W. C. Campbell, L.-M. Duan, Z.-X. Gong, A. V. Gorshkov, P. W. Hess, R. Islam, K. Kim, N. M. Linke, G. Pagano *et al.*, *Rev. Mod. Phys.* **93**, 025001 (2021).
- ¹⁷M. Saffman, T. G. Walker, and K. Mølmer, *Rev. Mod. Phys.* **82**, 2313 (2010).
- ¹⁸H. Levine, A. Keesling, A. Omran, H. Bernien, S. Schwartz, A. S. Zibrov, M. Endres, M. Greiner, V. Vuletić, and M. D. Lukin, *Phys. Rev. Lett.* **121**, 123603 (2018).
- ¹⁹F. Jelezko and J. Wrachtrup, *Phys. Status Solidi A* **203**, 3207 (2006).
- ²⁰M. W. Doherty, N. B. Manson, P. Delaney, F. Jelezko, J. Wrachtrup, and L. C. Hollenberg, *Phys. Rep.* **528**, 1 (2013).
- ²¹D. Loss and D. P. DiVincenzo, *Phys. Rev. A* **57**, 120 (1998).
- ²²J. R. Petta, A. C. Johnson, J. M. Taylor, E. A. Laird, A. Yacoby, M. D. Lukin, C. M. Marcus, M. P. Hanson, and A. C. Gossard, *Science* **309**, 2180 (2005).
- ²³Y. Nakamura, Y. A. Pashkin, and J. Tsai, *Nature* **398**, 786 (1999).
- ²⁴T. P. Orlando, J. E. Mooij, L. Tian, C. H. van der Wal, L. S. Levitov, S. Lloyd, and J. J. Mazo, *Phys. Rev. B* **60**, 15398 (1999).
- ²⁵K. Wright, K. M. Beck, S. Debnath, J. Amini, Y. Nam, N. Grzesiak, J.-S. Chen, N. Pimenti, M. Chmielewski, C. Collins *et al.*, *Nat. Commun.* **10**, 5464 (2019).
- ²⁶L. Egan, D. M. Debroy, C. Noel, A. Risinger, D. Zhu, D. Biswas, M. Newman, M. Li, K. R. Brown, M. Cetina, and C. Monroe, *Nature* **598**, 281 (2021).
- ²⁷C. Noel, P. Niroula, D. Zhu, A. Risinger, L. Egan, D. Biswas, M. Cetina, A. V. Gorshkov, M. J. Gullans, D. A. Huse, and C. Monroe, *Nat. Phys.* **18**, 760 (2022).
- ²⁸J. Zhang, G. Pagano, P. W. Hess, A. Kyprianidis, P. Becker, H. Kaplan, A. V. Gorshkov, Z.-X. Gong, and C. Monroe, *Nature* **551**, 601 (2017).
- ²⁹E. L. Hahn, *Phys. Rev.* **80**, 580 (1950).
- ³⁰L. Childress, M. V. G. Dutt, J. M. Taylor, A. S. Zibrov, F. Jelezko, J. Wrachtrup, P. R. Hemmer, and M. D. Lukin, *Science* **314**, 281 (2006).
- ³¹X. Rong, J. Geng, F. Shi, Y. Liu, K. Xu, W. Ma, F. Kong, Z. Jiang, Y. Wu, and J. Du, *Nat. Commun.* **6**, 8748 (2015).
- ³²Y. Chu, M. Markham, D. J. Twitchen, and M. D. Lukin, *Phys. Rev. A* **91**, 021801 (2015).
- ³³A. R. Milne, C. Hempel, L. Li, C. L. Edmunds, H. J. Slatyer, H. Ball, M. R. Hush, and M. J. Biercuk, *Phys. Rev. Lett.* **126**, 250506 (2021).
- ³⁴B. Gu and I. Franco, *J. Chem. Phys.* **151**, 014109 (2019).
- ³⁵A. J. Leggett, S. Chakravarty, A. T. Dorsey, M. P. Fisher, A. Garg, and W. Zwerger, *Rev. Mod. Phys.* **59**, 1 (1987).
- ³⁶P. L. Walters, T. C. Allen, and N. Makri, *J. Comput. Chem.* **38**, 110 (2017).
- ³⁷Z. Tong, X. Gao, M. S. Cheung, B. D. Dunietz, E. Geva, and X. Sun, *J. Chem. Phys.* **153**, 044105 (2020).
- ³⁸D. Xu and K. Schulten, *Chem. Phys.* **182**, 91 (1994).
- ³⁹Z. Hu, D. Brian, and X. Sun, *J. Chem. Phys.* **155**, 124105 (2021).
- ⁴⁰Y. Zhao, K. Sun, L. Chen, and M. Gelin, *WIREs Comput. Mol. Sci.* **12**, e1589 (2022).
- ⁴¹Y. Zhao, *J. Chem. Phys.* **158**, 080901 (2023).
- ⁴²N. Wu, L. Duan, X. Li, and Y. Zhao, *J. Chem. Phys.* **138**, 084111 (2013).
- ⁴³L. Wang, L. Chen, N. Zhou, and Y. Zhao, *J. Chem. Phys.* **144**, 024101 (2016).
- ⁴⁴L. Chen, M. Gelin, and Y. Zhao, *Chem. Phys.* **515**, 108 (2018).
- ⁴⁵Y. Zhang, E. Lötstedt, and K. Yamanouchi, *J. Phys. B-At. Mol. Opt.* **50**, 185603 (2017).
- ⁴⁶L. Chen, E. Palacino-González, M. F. Gelin, and W. Domcke, *J. Chem. Phys.* **147**, 234104 (2017).
- ⁴⁷T. N. Ikeda, S. Tanaka, and Y. Kayanuma, *Phys. Rev. Res.* **4**, 033075 (2022).
- ⁴⁸H. Wang, A. Marino, and J. Jing, *Appl. Phys. Lett.* **107**, 121106 (2015).
- ⁴⁹S. L. Braunstein and P. van Loock, *Rev. Mod. Phys.* **77**, 513 (2005).
- ⁵⁰J. Jing, J. Zhang, Y. Yan, F. Zhao, C. Xie, and K. Peng, *Phys. Rev. Lett.* **90**, 167903 (2003).
- ⁵¹T. Aoki, N. Takei, H. Yonezawa, K. Wakui, T. Hiraoka, A. Furusawa, and P. van Loock, *Phys. Rev. Lett.* **91**, 080404 (2003).
- ⁵²X. Su, A. Tan, X. Jia, J. Zhang, C. Xie, and K. Peng, *Phys. Rev. Lett.* **98**, 070502 (2007).
- ⁵³M. Yukawa, R. Ukai, P. van Loock, and A. Furusawa, *Phys. Rev. A* **78**, 012301 (2008).
- ⁵⁴G. Vathakkattil Joseph and V. Pakrashi, *Sci. Rep.* **10**, 10178 (2020).
- ⁵⁵D. A. Hite, Y. Colombe, A. C. Wilson, K. R. Brown, U. Warring, R. Jördens, J. D. Jost, K. S. McKay, D. P. Pappas, D. Leibfried, and D. J. Wineland, *Phys. Rev. Lett.* **109**, 103001 (2012).
- ⁵⁶M. Brownnutt, M. Kumph, P. Rabl, and R. Blatt, *Rev. Mod. Phys.* **87**, 1419 (2015).
- ⁵⁷J. A. Sedlacek, J. Stuart, D. H. Slichter, C. D. Bruzewicz, R. McConnell, J. M. Sage, and J. Chiaverini, *Phys. Rev. A* **98**, 063430 (2018).
- ⁵⁸J. Zeng, X.-T. Yan, Y. Yao, Y.-J. Zhao, L. Chen, and M. Feng, *Phys. Rev. A* **108**, 023121 (2023).
- ⁵⁹J. Keller, P.-Y. Hou, K. C. McCormick, D. C. Cole, S. D. Erickson, J. J. Wu, A. C. Wilson, and D. Leibfried, *Phys. Rev. Lett.* **126**, 250507 (2021).